PHM Framework for Discrete IGBTs in EV Applications: A PoF-Based Approach with a State-of-Damage Metric

JuHwan Kim[1], Junseop Lee[2], and Changwoon Han[3]

[1,2,3]*Department of Mechanical Engineering, SUNY Korea, Yeonsu-gu, Incheon, 21985, Republic of Korea*

juhwan.kim@stonybrook.edu
junseop.lee@stonybrook.edu
changwoon.han@sunykorea.ac.kr

ABSTRACT

Power converters are increasingly required to deliver higher power density and longer service life, which increases the need for accurate remaining useful life (RuL) prediction of their switching devices. Although module-type switching devices dominate many applications, discrete insulated-gate bipolar transistors (IGBTs) remain commercially important and are deployed in traction inverters, making robust lifetime prediction models (LPMs) for discrete devices directly relevant to prognostics and health management (PHM).

This paper presents a Physics-of-Failure (PoF)-based LPM for discrete IGBTs that models die-attach solder degradation as the dominant wear-out mechanism. A novel State-of-Damage (SoD) framework is further proposed to unify high- and low-cycle fatigue degradation within a single state variable, enabling damage accumulation under mixed-stress mission profiles. The proposed LPM and SoD metric are experimentally validated through power cycling tests.

The proposed approach provides a practical alternative to data-driven methods, which typically require extensive failure datasets and additional sensing or data acquisition hardware that are costly to obtain and often unavailable in industrial environments. By grounding RuL estimation in the dominant degradation mechanism, the framework remains computationally efficient and data-lean while enabling reliable health assessment and RuL prediction for discrete IGBT-based power electronic systems.

1. INTRODUCTION

Insulated-gate bipolar transistors (IGBTs) are widely used in power converters, making their reliability a critical determinant of system availability and safety, particularly in electric vehicle (EV) applications. IGBT reliability remains a persistent concern, motivating the need for a practical prognostics and health management (PHM) framework capable of accurately estimating remaining useful life (RuL) (Reimers et al. 2019; Yang et al. 2011). PHM approaches are generally classified into two categories: model-based and data-driven (Kim, An, and Choi 2017). Data-driven approaches typically rely on large volumes of failure data and additional sensing and data acquisition hardware, which can present a significant cost barrier in cost-sensitive industries such as the EV sector. Model-based approaches, in contrast, typically require two components: a lifetime prediction model (LPM) that links constant loading conditions to cycles-to-failure (N_f), and a cumulative damage model (CDM) that aggregates damage accumulated under varying loading conditions. The proposed framework combines these into a State-of-Damage (SoD) metric that quantifies the state of health in a steady and monotonic fashion. Relative to data-driven methods, model-based approaches reduce the need for extensive data collection and additional hardware investment.

For PHM applications, the SoD must evolve in a steady and monotonic manner; fluctuating or exponentially decreasing RuL predictions render maintenance planning unreliable (Lei et al. 2018). Existing SoD metrics such as Miner's rule are widely used for their simplicity but neglect load-sequence effects, which can be significant under variable loading (Miner 2021). Alternatives such as the Hashin–Rotem (HR) models better capture sequence sensitivity but treat high- and low-cycle stress as two separate formulations (Hashin and Rotem 1978). For EV traction inverters, where IGBTs experience mixed high- and low-cycle stress under complex variable loading, a unified SoD metric spanning both fatigue regimes is needed.

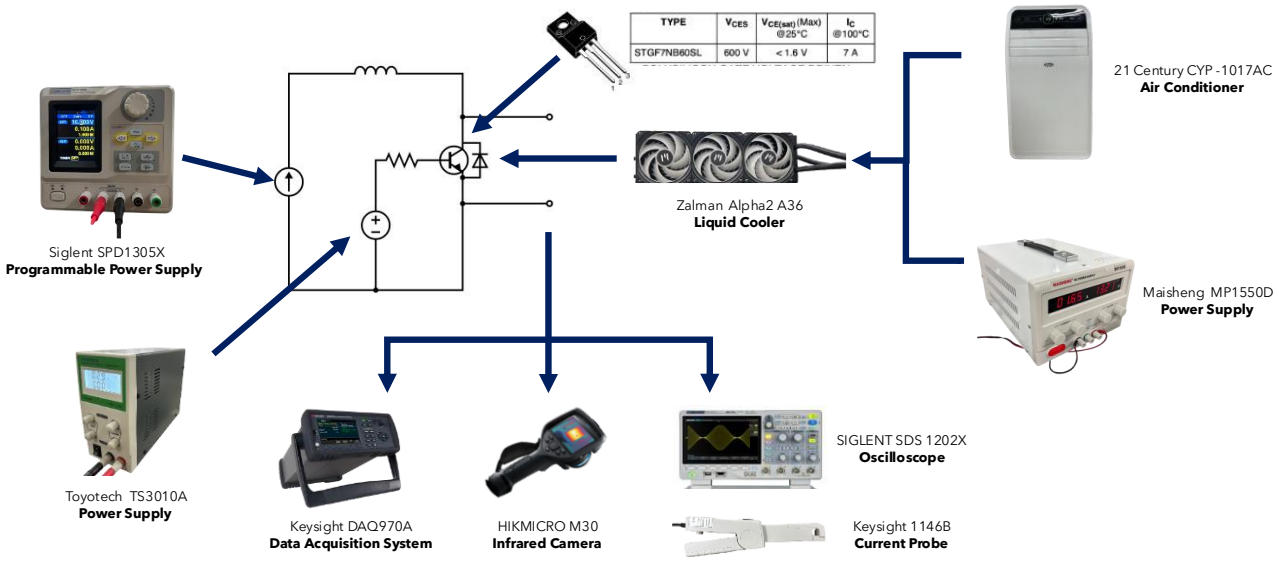

Figure 1. Schematic diagram of the experiment setup.

Most existing IGBT LPMs, including the LESIT, CIPS2008, and SEMIKRON models, are empirical and were developed primarily for module packages (Abuelnaga, Narimani, and Bahman 2021). Discrete IGBTs, despite their widespread deployment across the EV industry and other sectors, remain comparatively understudied. Module-based LPMs cannot be directly applied to discrete IGBTs due to their distinct dominant failure mechanisms, highlighting the need for an LPM developed specifically for discrete devices. In this context, PoF-based LPMs are promising candidates as they are grounded in physical degradation mechanisms rather than empirical correlation.

To address these gaps, this paper proposes a PHM framework for discrete IGBTs that integrates a PoF-based LPM with a unified SoD metric suitable for variable loading. The primary contributions are twofold: (i) the development of a Darveaux-based PoF LPM tailored to discrete IGBTs, and (ii) the derivation of a new SoD metric that unifies high- and low-cycle stress within a single state variable, enabling damage accumulation tracking under mixed and sequence-dependent load profiles. Compared with purely data-driven PHM frameworks, which typically require extensive failure data, the proposed framework is data-lean and requires only experimental data to calibrate the LPM.

2. PHYSICS-OF-FAILURE LIFETIME PREDICTION MODEL DEVELOPMENT

Development of a PoF-based LPM requires identification of the dominant failure mechanism governing device degradation. The primary failure mechanisms of IGBTs are solder layer fatigue and bond-wire degradation (Scheuermann and Schmidt 2013). Both are driven by mismatches in the coefficient of thermal expansion (CTE) among the constituent materials, which induce stresses at the material interfaces. Both mechanisms have been widely studied, and bond-wire degradation is often reported as the governing wear-out mechanism for IGBTs. For the specific DUTs tested in this study, however, scanning acoustic microscopy (SAM) evidence (presented in the Experimental Results section) shows die-attach solder degradation as the observed failure mode. On this basis, solder layer fatigue is adopted as the failure mechanism of interest in this study.

To quantify solder fatigue, the Darveaux energy-based model is employed (Darveaux 2002). The Darveaux model postulates that thermomechanical fatigue life is governed by the inelastic strain energy density per cycle (ΔW). Because local stress and strain values are highly mesh-sensitive near geometric discontinuities, the volume-averaged ΔW (ΔW_{avg}) across the solder layer is used. Solder fatigue lifetime is decomposed into two phases: crack initiation and propagation. The Darveaux model is expressed as,

$$N_f = N_0 + \frac{a}{da/dN}, \tag{1}$$

where N_0 is cycles to crack initiation, $\frac{da}{dN}$ is crack propagation rate, and a is the characteristic length. N_0 and $\frac{da}{dN}$ are given as:

$$N_0 = K_1 \Delta W_{avg}^{K_2}, \tag{2}$$

$$\frac{da}{dN} = K_3 \Delta W_{avg}^{K_4}, \tag{3}$$

where $K_1 - K_4$ are material-specific constants.

By establishing a physically grounded relationship between ΔW_{avg} and N_f, the Darveaux model provides a robust framework for predicting die-attach solder joint lifetime.

2.1. Experimental Design

To calibrate the proposed PoF-based LPM, a series of accelerated life tests (ALTs) was designed to isolate and characterize the dominant solder degradation mechanism. A schematic of the experimental setup is shown in Fig. 1.

The device under test (DUT) selected for this study is a TO-220 package IGBT (STGF7NB60SL). This device does not incorporate an internal freewheeling diode, eliminating a secondary source of power dissipation, simplifying the thermal loading conditions. The die-attach layer employs 95.5Pb2Sn2.5Ag, commercially known as Indalloy 163, a high-melting-temperature solder widely used in power semiconductor devices. Despite its wide adoption, the reliability behavior of this high-lead alloy has received limited attention relative to lead-free alternatives such as SAC305, making it a suitable candidate for this investigation.

The ALTs were implemented on a DC power cycling testbed to induce cyclic thermomechanical stress on the solder layer. To achieve a large junction temperature swing (ΔT_j) while maintaining low current levels, a reduced gate voltage (V_{GE}) of 2.9 V was applied, placing the IGBT in a partially turned-on state slightly above the threshold voltage. This increases the effective channel resistance and, consequently, power dissipation within the device (Patil et al. 2009). During testing, the load current was the sole parameter varied, ranging from 4 A to 5 A. This directly controlled the applied ΔT_j, yielding values between 65 K and 130 K and, by extension, governing ΔW_{avg}. The heating time (t_{on}) and cooling time (t_{off}) were fixed at 1 s and 7.5 s, respectively, across all tests.

The setup employs two power supplies to provide the sensing current, load current, and V_{GE}. The DUT is mounted on a liquid cooler powered by a separate supply and coupled with an air conditioning unit, maintaining the heatsink temperature at $18\,^{\circ}\mathrm{C} \pm 0.5\,^{\circ}\mathrm{C}$ throughout the tests. This ensures repeatable test conditions and simplifies the thermal boundary definitions for the subsequent finite element analysis (FEA). Electrical and thermal measurements are continuously acquired using a DAQ system, an oscilloscope, an infrared (IR) camera, and a current probe.

A key advantage of DC power cycling is continuous monitoring of degradation parameters such as the collector-emitter on-state voltage ($V_{CE,on}$) (Abuelnaga et al. 2021). $V_{CE,on}$ is used to compute the junction-to-case thermal resistance (R_{th}), an indicator of solder layer degradation. In this study, a 20% increase in R_{th} was adopted as the initial end-of-life (EOL) degradation indicator. In addition, $V_{CE,on}$ serves as a temperature-sensitive electrical parameter (TSEP) for monitoring the junction temperature (T_j). At a fixed sensing current of 100 mA and V_{GE} of 2.9 V, experimental calibration established a linear relation in which a 1.6 mV decrease in $V_{CE,on}$ corresponds to a $1\,^{\circ}\mathrm{C}$ increase in T_j, enabling accurate, non-intrusive temperature tracking.

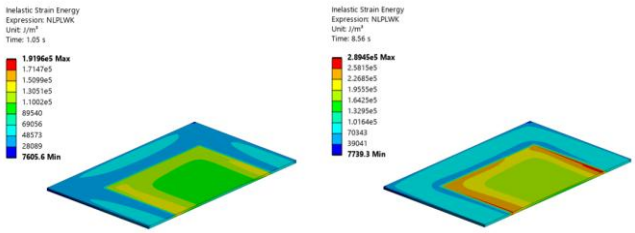

a) b)

Figure 2. Strain energy density distribution in the solder joint at the end of the a) heating and b) cooling phases during the static structural simulation.

2.2. Strain Energy Density Evaluation

FEA was performed to simulate the transient temperature and stress fields during power cycling and to compute ΔW_{avg} to calibrate the proposed LPM.

To capture time- and temperature-dependent solder deformation, the Anand viscoplastic constitutive model was employed. The Anand model represents both plasticity and creep within a unified formulation, making it well-suited for high-temperature solder analysis (Anand 1985). Because Anand parameters for 95.5Pb2Sn2.5Ag are not available in the open literature, properties from a closely related high-lead solder (92.5Pb5Sn2.5Ag) were adopted. This substitution is supported by the comparable density, tensile strength, and CTE of the two alloys.

Thermal boundary conditions were defined to replicate the experimental setup. A constant-temperature boundary condition was applied to the bottom surface of the device, consistent with the stable heatsink temperature observed during testing. Heat generation on the silicon chip was prescribed from the measured time-varying power profile derived from in-situ current and voltage readings. Convection and radiation from the top surfaces were neglected, as conduction through the baseplate dominates heat transfer in this configuration.

ΔW_{avg} was computed in two stages. First, a transient thermal simulation was performed and validated against both IR and TSEP measurements. This dual validation is a distinguishing feature of the present workflow: the maximum junction temperature was obtained from the TSEP method and the surface temperature distribution from IR imaging, providing two independent references rather than one. Because ΔW_{avg} cannot be measured directly, this agreement with two independent measurements, within 2.2% for the T_j and 1.8% for the surface temperature, reduces the likelihood that an

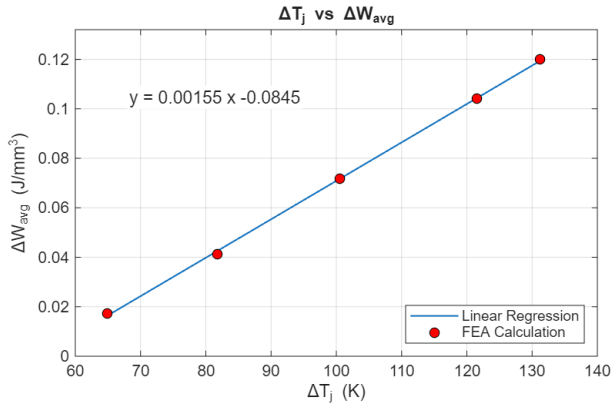

Figure 3. Relationship between ΔW_{avg} and ΔT_j.

undetected error propagates into the computed strain energy and supports the fidelity of the calculated value.

The resulting temperature history was then applied as a thermal load in a thermomechanical simulation to compute the strain energy shown in Fig. 2. A mesh refinement study confirmed that ΔW_{avg} stabilized at approximately one million nodes, whereas the localized maximum strain energy did not converge even at five million nodes.

Because the Anand model is rate-dependent, time discretization was also controlled. The cooling phase ($t_{off} = 7.5s$) converged at 80 steps, while the heating phase ($t_{on} = 1s$) required 176 steps to balance computational cost against a 5% convergence tolerance. Four complete power cycles were simulated to stabilize the stress-strain hysteresis loop. As shown in Fig. 3, the FEA results exhibit a predominantly linear relationship between the applied ΔT_j and the corresponding ΔW_{avg}, attributable to the short t_{on} that limits non-linear creep. This relationship was used to approximate ΔW_{avg} for each DUT at reduced computational cost.

2.3. Experimental Results

While a 20% increase in R_{th} served as the initial degradation marker, catastrophic device failure (complete loss of switching functionality) was adopted as the final EOL criterion to ensure an unambiguous termination point. Degradation was continuously monitored using $V_{CE,on}$, enabling observation of pre-failure trends.

A total of 20 DUTs were power cycled to EOL to establish the lifetime dependence on ΔW_{avg}. Although the loading profiles targeted nominal ΔT_j levels of 75, 100, and 130 K, device-to-device variability produced measured ΔT_j values spanning 65 K – 130 K. The resulting N_f ranged from 4,901 to 388,534 cycles and exhibited a strong linear decrease with increasing ΔW_{avg} on a log–log scale.

To identify the dominant wear-out mechanism, SAM analysis was conducted on unaged and EOL DUTs, as shown in Fig. 4. The unaged samples exhibited a uniform acoustic response, whereas the EOL devices showed pronounced dark regions indicative of cracks and delamination within the die-attach solder layer (Liu et al. 2024), indicating solder fatigue as the dominant failure mode for the tested DUTs.

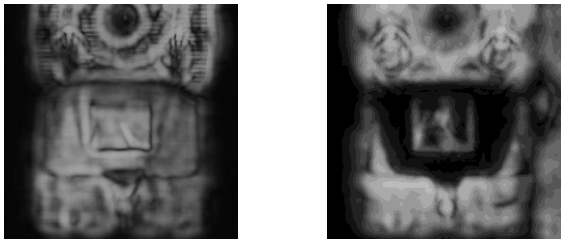

a) b)

Figure 4. SAM T-scan images comparing a) a healthy DUT with b) an EOL DUT, with darker areas indicating damage which show extensive solder degradation.

Table 1. LPM parameters for 95.5Pb2Sn2.5Ag.

Solder	K_3	K_4
92.5Pb5Sn2.5Ag	0.05321	2.012

2.4. Lifetime Prediction Model Formulation

The proposed LPM assumes that device lifetime is governed primarily by the crack propagation phase. Inherent solder joint defects such as voids and flux residues act as stress concentrators and effectively serve as pre-existing crack initiation sites (Hu et al. 2021). Consequently, stable crack growth dominates the low-cycle fatigue life characteristic of power cycling. Using published Darveaux constants for comparable solders such as SAC305, Eq. 2 predicts that the crack initiation phase for this DUT at ΔT_j=130 K accounts for less than 2% of the total lifetime, confirming that device life is dominated by propagation.

The experimental N_f were paired with the corresponding computed ΔW_{avg}, and the propagation-based LPM was calibrated by least-squares linear regression in log–log space, yielding the crack growth multiplier and exponent. With these fitted constants summarized in Table 1, the calibrated LPM for the discrete IGBT is expressed as,

$$N_f = \frac{a}{0.05321 \cdot (\Delta W_{avg})^{2.012}} \quad (4)$$

where a denotes the effective crack length at EOL, measured to be 4 mm for this DUT geometry.

Predictions of the proposed LPM are compared with experimental data and with predictions of existing LPMs in Fig. 5. For example, at ΔT_j=77.92 K, the proposed LPM

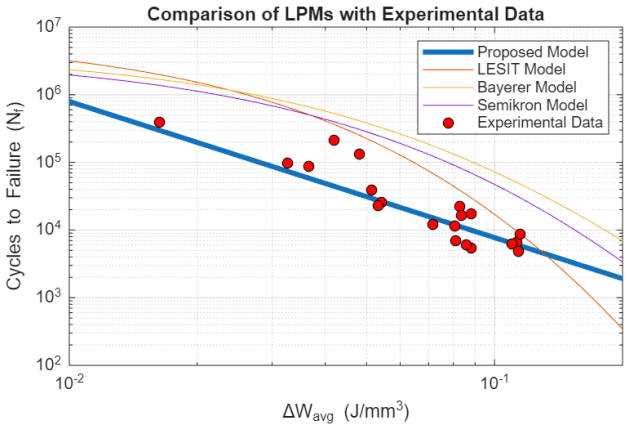

Figure 5. Comparison of predicted lifetimes from the proposed LPM and statistical ones against the experimental data.

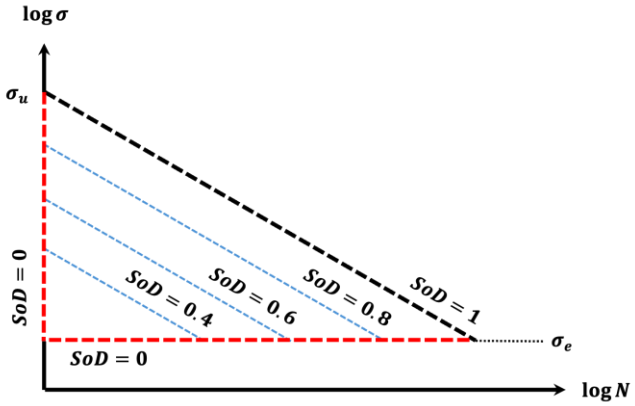

Figure 6. Visualization of Miner's Rule highlighting multiple stress levels arbitrarily contributing to initial SoD.

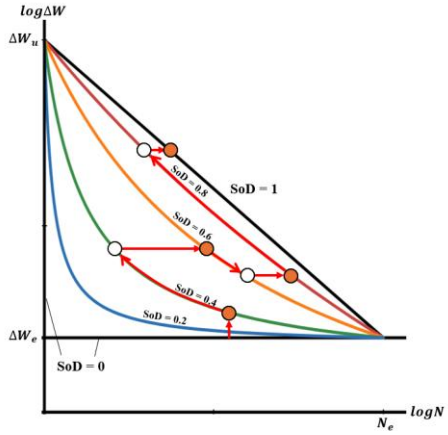

Figure 7. Illustration of isodamage curves and the growth of SoD along the curves.

predicts 58,371 cycles, in close agreement with the measured value of 87,137 cycles, whereas the LESIT, CIPS2008, and SEMIKRON models predict non-conservative lifetimes of 516,774, 659,709, and 508,693 cycles, respectively, overestimating measured life by roughly an order of magnitude. This gap reflects a mismatch in the assumed failure mechanism: the module-based models are calibrated against bond-wire fatigue, whereas the DUTs in this study exhibit die-attach solder fatigue. Applying module-based LPMs to discrete devices with a different dominant mechanism can therefore yield non-conservative life estimates, motivating a PoF LPM that is tied to the mechanism actually observed.

3. STATE-OF-DAMAGE METRIC DEVELOPMENT

3.1. Available SoD Metrics

Miner's rule is the most widely used SoD approach for estimating cumulative damage but does not account for load-sequence effects. This limitation is evident on an SoD diagram (Fig. 6), where $SoD = 1$ is defined by an LPM: Miner's rule exhibits boundary inconsistencies at $SoD = 0$ (at $N = 1$ and where the applied stress equals the endurance limit, σ_e), where multiple stress levels contribute arbitrarily to the initial SoD.

Alternative SoD models such as the HR models address the sequence limitation of Miner's rule by employing isodamage lines that converge at "knee points" with distinct relative slopes (Hashin and Rotem 1978). These models are separated by fatigue regime: the HR endurance limit (HR-S_e) and ultimate strength (HR-S_u) formulations apply to high- and low-cycle fatigue, respectively, and are restricted to applications in which high and low load levels are clearly separated.

Previous studies have proposed conceptual isodamage curves that unify high- and low-cycle fatigue isodamage-line models within a single framework (Bjørheim, Pavlou, and Siriwardane 2022; Pavlou 2018). However, these formulations are not directly applicable to PHM because the resulting damage can fluctuate or grow exponentially.

3.2. Proposed SoD Metric

The proposed damage model extends the isodamage concept by unifying the distinct knee-point formulations into explicit mathematical expressions, enabling direct computation of SoD.

As shown in Fig. 7, the isodamage curves are defined on an SoD domain bounded by SoD=0 and SoD=1, plotted on a log–log scale with ΔW assigned as the ordinate.

For the proposed model, a rational function that is concave upward and constrained by normalized intercepts at (1,0) and (0,1) is employed as the core equation,

$$y = \frac{1-x}{1+ax} \text{ where } a \geq 0. \quad (5)$$

This form was chosen because it naturally enforces the required boundary conditions - zero damage at zero cycles and complete failure at $SoD = 1$ - and a serves as a shape factor controlling the curvature of the isodamage curve at load step k. It further ensures that the function lies entirely beneath the LPM curve in the first quadrant while preserving algebraic simplicity.

To apply this to solder fatigue, the normalized coordinates are mapped to the physical LPM plane on a log-log scale, with y and x corresponding to ΔW_{avg} and the number of cycles, respectively. Incorporating the material's physical properties-such as the endurance limit and ultimate strength-and the cumulative number of applied cycles at load step k transforms the normalized equation into the physical domain,

$$log\left(\frac{\Delta W_k}{\Delta W_e}\right) = B\left[\frac{log\left(\frac{N_e}{n_{k-1@k}+n_k}\right)}{1+a_k\, log(n_{k-1@k}+n_k)}\right], \quad (6)$$

$$\text{where } B = -\frac{log\left(\frac{\Delta W_u}{\Delta W_e}\right)}{log(N_e)} \quad (7)$$

$$n_{k-1@k} = 10^{\left[\frac{log(N_e)-\frac{log\left(\frac{\Delta W_k}{\Delta W_e}\right)}{B}}{1+\frac{log\left(\frac{\Delta W_k}{\Delta W_e}\right)}{B}a_{k-1}}\right]}, \quad (8)$$

$$\text{and } a_k = \frac{B\, log\left(\frac{N_e}{n_{k-1@k}+n_k}\right)-log\left(\frac{\Delta W_k}{\Delta W_e}\right)}{log\left(\frac{\Delta W_k}{\Delta W_e}\right) log(n_{k-1@k}+n_k)}, \quad (9)$$

where ΔW_k, ΔW_e, and ΔW_u denote ΔW at the load step k, the endurance limit, and the ultimate strength, respectively, N_e is the N_f at the endurance limit, n_k is the number of applied cycles at the load step k, $n_{k-1@k}$ is equivalent to n_{k-1} at load level k, and a_k is the shape factor.

Higher values of a_k correspond to lower accumulated damage, drawing the isodamage curve closer to the axes; lower values of a_k correspond to higher accumulated damage, pushing the curve toward the LPM curve.

3.2.1. SoD_C

Based on these derivations, the proposed SoD model can be formulated as SoD curve, or SoD_C. This SoD_C formulation is analogous to Miner's rule, which states that damage is measured by the cycle ratio of the number of applied cycles at load level k to the N_f at that load level:

$$SoD_C = \frac{n_k + n_{k-1@k}}{N_k} = \frac{n_k + 10^{\left[\frac{log(N_e)-\frac{log\left(\frac{\Delta W_k}{\Delta W_e}\right)}{B}}{1+\frac{log\left(\frac{\Delta W_k}{\Delta W_e}\right)}{B}a_{k-1}}\right]}}{10^{\left[log(N_e)-\frac{log\left(\frac{\Delta W_k}{\Delta W_e}\right)}{B}\right]}}, \quad (10)$$

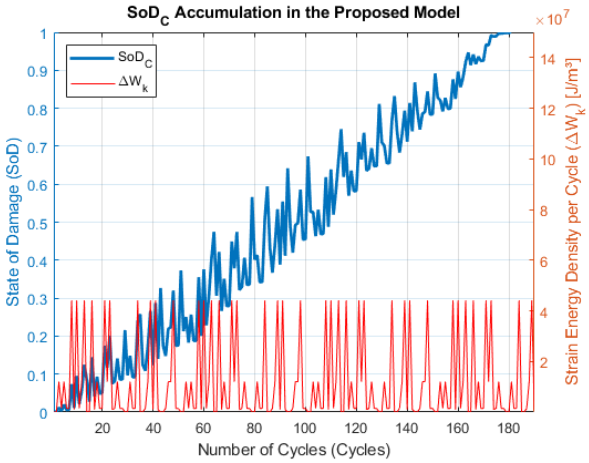

a) SoD_C

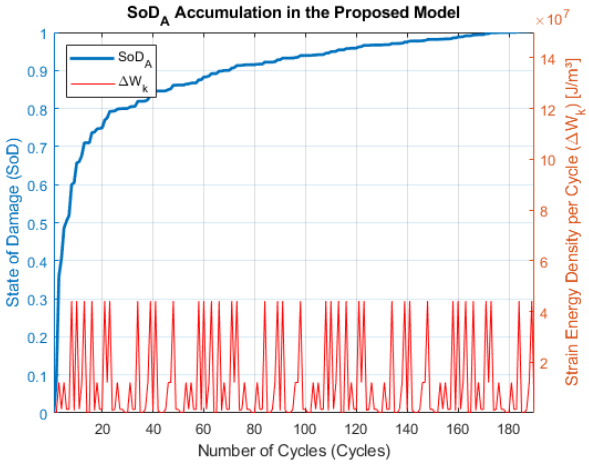

b) SoD_A

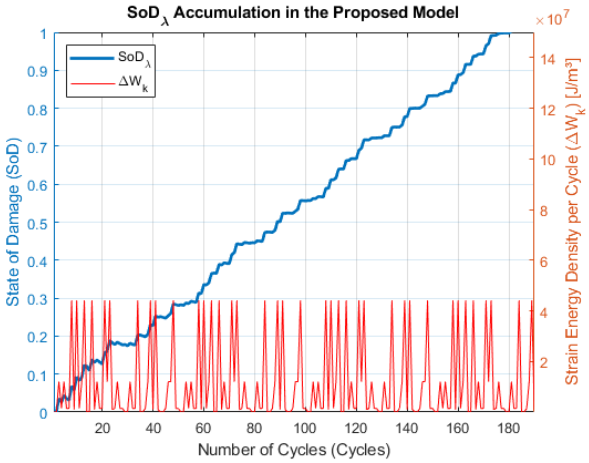

c) SoD_λ

Figure 8. Accumulation of damage over variable loading cycles using the proposed a) SoD_C, b) SoD_A, and c) SoD_λ.

where N_k is the N_f at load level k. However, as shown in Fig. 8(a), SoD_C does not exhibit monotonic behavior but instead fluctuates.

3.2.2. SoD_A

To address the fluctuation observed in SoD_C of Eq. 10, an area-based SoD definition, denoted SoD_A, is introduced. This formulation is motivated by the observation that a_k decreases monotonically as damage accumulates. SoD_A is defined as the ratio of the area under the isodamage curve at load step k to the total area at failure,

$$SoD_A = \frac{A_k}{A_F}, \tag{11}$$

where A_k is the area under the curve and A_F is the total area at failure. A_k can be calculated by taking the integral of the curve equation over the range of 1 to 10 in log-log scale, which makes the integration with respect to $\log(n_{k-1@k} + n_k)$ over the range of $\log(1)$ to $\log(10)$,

$$A_k = \int_{log(1)}^{log(N_e)} log\left(\frac{\Delta W_k}{\Delta W_e}\right) d(log\, n_{k-1@k} + n_k). \tag{12}$$

A_F, which defines the area under the life prediction curve, can be calculated by the area at $a_k = 0$. Taking the limit $a_k \to 0$,

$$A_F = \lim_{a_k \to 0} A_k = \frac{B}{2}[log(N_e)]^2. \tag{13}$$

Therefore, SoD_A is expressed by,

$$SoD_A = \frac{2[-a_k\, log(N_e) + (a_k\, log(N_e) + 1)\, ln(a_k\, log(N_e) + 1)]}{a_k^2[log(N_e)]^2}. \tag{14}$$

SoD_A is plotted over time in Fig. 8(b), confirming that local fluctuations are suppressed. However, damage accumulation is not monotonic but grows exponentially: SoD_A rises sharply in early life, compressing most of the observable degradation into a short interval. This exponential growth results from the rapid decrease of a_k toward zero.

3.2.3. SoD_λ

Similar behaviors have been reported in previous studies (Lee, Park, and Han 2024), where an exponential scale factor λ was introduced to reconcile the fluctuations of SoD_C with the exponential growth of SoD_A. The same approach is applied here by introducing λ to SoD_A:

$$SoD_\lambda = SoD_A^\lambda, \tag{15}$$

$$\lambda = \frac{1}{k}\sum_1^k \frac{log(SoD_C)}{log\,(SoD_A)} = \frac{1}{k}\sum_1^k \frac{log\left(\frac{n_k + n_{k-1@k}}{N_k}\right)}{log\,(\frac{A_k}{A_F})}. \tag{16}$$

When SoD_λ was plotted over time under the same loading conditions as those used for the other SoD definitions (Fig. 8(c)), it exhibits both monotonic and steady growth, confirming the suitability of SoD_λ for PHM applications.

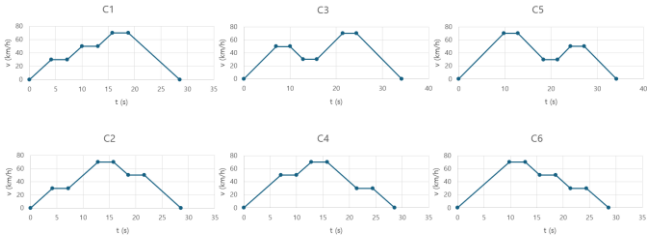

Figure 9. Simplified driving cycle profiles C1 to C6 with randomized variations.

Table 2. Driving scenarios from S1 to S5, emphasizing the variable loading conditions

Scenario	Sequence
S1	C1-C2-C3-C4-C5-C6
S2	C3-C6-C1-C5-C2-C4
S3	C6-C2-C5-C3-C4-C1
S4	C2-C4-C6-C1-C3-C5
S5	C5-C1-C3-C2-C6-C4

4. EXPERIMENTAL VALIDATION

The proposed SoD metric was validated using ALTs similar to those used for LPM calibration but conducted under complex variable loading conditions.

4.1. Mission Profile Development

Although standardized driving cycles exist, simplified cycles were developed based on three representative road categories in South Korea: residential, urban, and rural—with target speeds of 30, 50, and 70 km/h, respectively, consistent with the regulated speed limits.

Velocity segments for each road category were sequentially connected and randomized to reflect the stochastic nature of real-world driving, producing six complete driving cycle profiles shown in Fig. 9. From these six profiles, five driving scenarios were assembled for the power cycling tests, as summarized in Table 2. The MATLAB-based Advanced Vehicle Simulator (ADVISOR) was then used to convert the scenarios into electrical loads.

4.2. Experimental Validation Results

A total of 10 DUTs were subjected to the power cycling ALT. Measured lifetimes ranged from 15,435 to 79,678 cycles, with most between 20,000 and 60,000 cycles, reflecting device-to-device manufacturing variability.

The corresponding Weibull distribution (Fig. 10) yields a mean time to failure (MTTF) of 40,715 cycles and a shape parameter of 2.22, indicating wear-out failure.

Figure 11 shows the evolution of the proposed SoD metrics under variable loading. All three formulations predict EOL at 36,349 cycles, corresponding to a 10.7% error relative to the experimental MTTF. However, only SoD_λ exhibits steady and monotonic growth under stochastic loading. By combining monotonic damage evolution with accurate life prediction, SoD_λ is well suited as a practical indicator for PHM applications.

These results clarify why the three formulations, despite sharing an identical end-of-life prediction, differ in their suitability for health monitoring. SoD_C is non-monotonic, which violates the irreversibility of fatigue damage. SoD_A removes these fluctuations but concentrates most of its growth within the early portion of life, leaving little resolution to distinguish a healthy device from one approaching failure. Only the scaled formulation preserves both monotonicity and a steady growth rate across the entire lifetime, the two properties required for continuous remaining-useful-life tracking. This comparison adds to existing knowledge in two respects. First, it converts the previously conceptual unified-isodamage representation into an explicit, closed-form metric that can be computed directly at each load step. Second, it demonstrates, under stochastic mission-profile loading rather than simple variable loading sequences, that accurate EOL prediction and a physically admissible damage trajectory can be obtained simultaneously. The practical implication is that the proposed metric can be evaluated from mission-profile stress histories alone, without the failure datasets or additional sensing hardware required by data-driven prognostics.

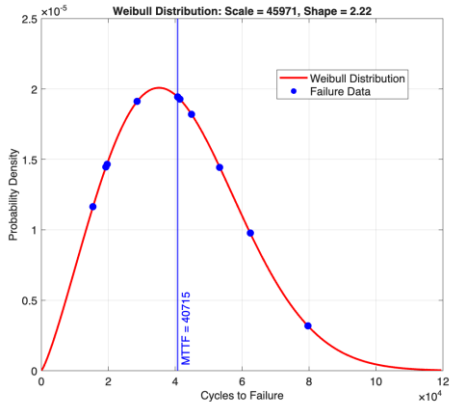

Figure 10. Weibull distribution of failure cycles with shape parameter of 2.22 and MTTF of 40,715 cycles.

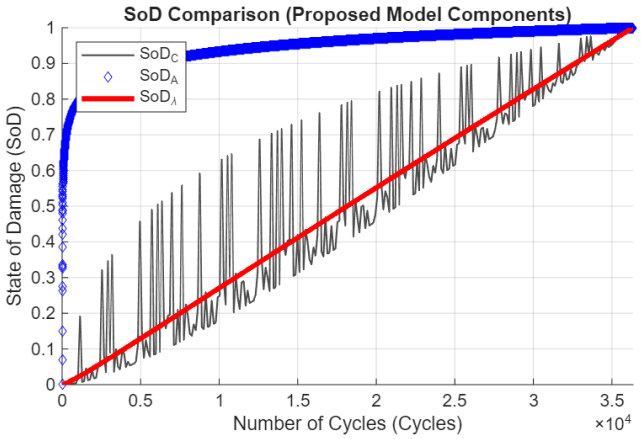

Figure 11. Comparison of the accumulation of SoD for different models over time.

5. CONCLUSION

This paper presented a PHM framework for discrete IGBTs integrating a PoF-based LPM with a new SoD metric.

First, a PoF-based LPM tailored to discrete IGBTs was developed. Die-attach solder fatigue was identified as the dominant wear-out mechanism; the LPM was formulated from the Darveaux model and calibrated against experimental data. The calibrated LPM predicted lifetimes consistent with the measurements, for example 58,371 cycles against a measured 87,137 cycles at a junction-temperature swing of 77.92 K, whereas the module-based LESIT, CIPS2008, and SEMIKRON models overestimated life by roughly an order of magnitude.

Second, a new SoD metric was proposed to enable damage accumulation under variable loading and was validated using ALTs designed to replicate complex EV driving cycles. The metric unifies high- and low-cycle fatigue within a single state variable while capturing load-sequence sensitivity. The proposed SoD_λ exhibits monotonic and steady damage evolution and predicts EOL within 10.7% of the experimental MTTF. The specific contribution is an explicit, closed-form damage metric that remains both monotonic and steady under stochastic mission-profile loading. By pairing a PoF-based LPM with a physically admissible health indicator, the framework enables RuL estimation for discrete IGBTs without large datasets required by data-driven methods. Extension of the framework to other discrete devices and solder systems remains a subject for future work.

ACKNOWLEDGEMENT

This work was supported in part by the National Research Foundation of Korea (NRF). (Project No. RS-2024-00336813139821778401 02).

REFERENCES

Abuelnaga, Ahmed, Mehdi Narimani, and Amir Sajjad Bahman. 2021. “A Review on IGBT Module Failure Modes and Lifetime Testing.” *IEEE Access* 9:9643–63. doi:10.1109/ACCESS.2021.3049738.

Anand, Lallit. 1985. "Constitutive Equations for Hot-Working of Metals." *International Journal of Plasticity* 1(3):213–31. doi:https://doi.org/10.1016/0749-6419(85)90004-X.

Bjørheim, Fredrik, Dimitrios G. Pavlou, and Sudath C. Siriwardane. 2022. "Nonlinear Fatigue Life Prediction Model Based on the Theory of the S-N Fatigue Damage Envelope." *Fatigue & Fracture of Engineering Materials & Structures* 45(5):1480–93. doi:10.1111/ffe.13680.

Darveaux, Robert. 2002. "Effect of Simulation Methodology on Solder Joint Crack Growth Correlation and Fatigue Life Prediction." *Journal of Electronic Packaging* 124(3):147–54. doi:10.1115/1.1413764.

Hashin, Z., and A. Rotem. 1978. "A Cumulative Damage Theory of Fatigue Failure." *Materials Science and Engineering* 34(2):147–60. doi:10.1016/0025-5416(78)90045-9.

Hu, Borong, Sylvia Konaklieva, Nadia Kourra, Mark A. Williams, Li Ran, and Wei Lai. 2021. "Long-Term Reliability Evaluation of Power Modules With Low Amplitude Thermomechanical Stresses and Initial Defects." *IEEE Journal of Emerging and Selected Topics in Power Electronics* 9(1):602–15. doi:10.1109/JESTPE.2019.2958737.

Kim, Nam-Ho, Dawn An, and Joo-Ho Choi. 2017. *Prognostics and Health Management of Engineering Systems*. Cham: Springer International Publishing.

Lee, Suyeon, Seungil Park, and Changwoon Han. 2024. "Prognostics and Health Management Using Nonlinear Cumulative Damage Model for Electronic Devices Under Variable Loading." *IEEE Access* 12:3356–71. doi:10.1109/ACCESS.2023.3347780.

Lei, Yaguo, Naipeng Li, Liang Guo, Ningbo Li, Tao Yan, and Jing Lin. 2018. "Machinery Health Prognostics: A Systematic Review from Data Acquisition to RUL Prediction." *Mechanical Systems and Signal Processing* 104:799–834. doi:10.1016/j.ymssp.2017.11.016.

Liu, Shenyi, Vesa Vuorinen, Xing Liu, Olli Fredrikson, Sebastian Brand, Nikhilendu Tiwary, Josef Lutz, and Mervi Paulasto-Kröckel. 2024. "Fatigue Crack Networks in Die-Attach Layers of IGBT Modules Under a Power Cycling Test." *IEEE Transactions on Power Electronics* 39(12):16695–707. doi:10.1109/TPEL.2024.3447909.

Miner, Milton A. 2021. "Cumulative Damage in Fatigue." *Journal of Applied Mechanics* 12(3):A159–64. doi:10.1115/1.4009458.

Patil, Nishad, Jose Celaya, Diganta Das, Kai Goebel, and Michael Pecht. 2009. "Precursor Parameter Identification for Insulated Gate Bipolar Transistor (IGBT) Prognostics." *IEEE Transactions on Reliability* 58(2):271–76. doi:10.1109/TR.2009.2020134.

Pavlou, Dimitrios G. 2018. "The Theory of the S-N Fatigue Damage Envelope: Generalization of Linear, Double-Linear, and Non-Linear Fatigue Damage Models." *International Journal of Fatigue* 110:204–14. doi:10.1016/j.ijfatigue.2018.01.023.

Reimers, John, Lea Dorn-Gomba, Christopher Mak, and Ali Emadi. 2019. "Automotive Traction Inverters: Current Status and Future Trends." *IEEE Transactions on Vehicular Technology* 68(4):3337–50. doi:10.1109/TVT.2019.2897899.

Scheuermann, U., and R. Schmidt. 2013. "Impact of Load Pulse Duration on Power Cycling Lifetime of Al Wire Bonds." *Microelectronics Reliability* 53(9):1687–91. doi:10.1016/j.microrel.2013.06.019.

Yang, Shaoyong, Angus Bryant, Philip Mawby, Dawei Xiang, Li Ran, and Peter Tavner. 2011. "An Industry-Based Survey of Reliability in Power Electronic Converters." *IEEE Transactions on Industry Applications* 47(3):1441–51. doi:10.1109/TIA.2011.2124436.